Structure, Energetics, and Dynamics of Screw Dislocations in Even *n*-Alkane Crystals

Isabel A. Olson,[1] Alexander G. Shtukenberg,[1] Gagik Hakobyan,[1] Andrew L. Rohl,[2] Paolo Raiteri,[2]* Michael D. Ward,[1]* Bart Kahr[1,3]**

[1] Department of Chemistry and Molecular Design Institute, New York University, New York City, NY, 10003, USA. [2]Curtin Institute for Computation and Department of Chemistry, Curtin University, P.O. Box U1987, Perth, Western Australia, 6845, Australia. [3]Graduate School of Advanced Science and Engineering (TWIns), Waseda University, Tokyo, Japan

Corresponding Authors

* bart.kahr@nyu.edu

*mdw3@nyu.edu

*p.raiteri@curtin.edu.au

*andrew.rohl@curtin.edu.au

ABSTRACT

Spiral hillocks on *n*-alkane crystal surfaces were observed immediately after Frank recognized the importance of screw dislocations for crystal growth, yet their structures and energies in molecular crystals remain ill-defined. To illustrate the structural chemistry of screw dislocations that are responsible for plasticity in organic crystals and upon which the organic electronics and pharmaceutical industries depend, molecular dynamics was used to examine heterochiral dislocation pairs with Burgers vectors along [001] in *n*-hexane, *n*-octane, and *n*-decane crystals. The cores were anisotropic and elongated in the (110) slip plane, with significant local changes in molecular position, orientation, conformation, and energy. This detailed atomic level picture produced a distribution of strain consistent with linear elastic theory, giving confidence in the simulations. Dislocations with doubled Burgers vectors split into pairs with elementary displacements. These results suggest a pathway to understanding the mechanical properties and failure associated with elastic and plastic deformation in soft crystals.

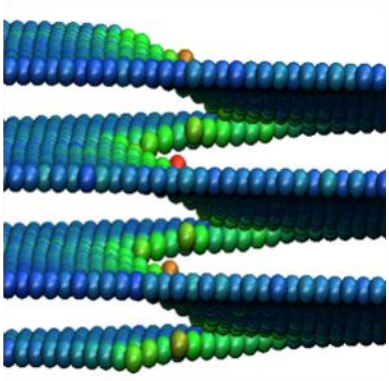

As the organic diodes and transistors of the flexible phones that will soon populate the modern world inevitably fail,[1] or when new active pharmaceutical ingredients resist tableting[2] – seemingly unrelated concerns for the materials scientist – attention will increasingly focus on the structures, energies, and origins of defects in crystals built from molecules that are responsible for plasticity.[3,4,5,6,7,8] Computation[9,10] and transmission electron microscopy[11,12] have revealed structures of dislocation cores in metals and binary solids in atomic detail, but despite this progress, molecular crystals remain for the most part *terra incognita*. Isolated computational excursions into this unexplored and more complex territory include the study of edge dislocations in naphthalene[13] as well as shear and slip structures in organic explosives.[14,15,16,17,18] Screw dislocations have been modeled in polyethylene,[19,20] C_{60},[21] RDX,[22] anthracene,[23] sucrose,[24] and acetaminophen,[24,25,26] the latter as part of a concerted program to model such structures in increasingly complex systems.[27,28,29,30,31] However, unlike 'hard' metals and minerals, dislocations in organic materials can not at present be imaged in molecular detail and evaluation of computed models must rely on structures that are chemically, energetically, and crystallographically sensible, and be consistent with the continuum elastic theory. Another distinctive feature of molecular crystals is coexistence of strong intramolecular and weak intermolecular forces that direct formation of specific supramolecular assemblies. For these reasons, the structural chemistry of dislocations in molecular materials must build systematically from the simple to the complex, just as molecular crystal structure based on the close packing principle is often logically presented through comparison of homologous long chain aliphatic compounds and polycyclic aromatic hydrocarbons.[32]

Herein, we begin populating the vacant space of systematic knowledge by describing the dynamics, structures, sizes, and core energetics of screw dislocations in even *n*-alkanes that are appealing for the following reasons: (*i*) images of well defined spiral hillocks on the (001) face of long *n*-alkanes, $C_{34}H_{70}$,[33] $C_{36}H_{74}$,[34,35] $C_{39}H_{80}$,[36] $C_{40}H_{82}$,[37] and $C_{100}H_{202}$,[38] have been reported; (*ii*) crystal structures of related smaller ($< C_{26}$) even *n*-alkanes are simple, crystallizing in the triclinic $P\bar{1}$ space group (Z=1) with only translational

symmetry between molecules in all-*anti* zigzag conformations (Fig. 1A);[39] (*iii*) long-chain molecules in crystals with Burgers vectors having large components in the long directions can produce large distortions; and (*iv*) conformational analysis and intermolecular interactions in paraffins are well understood.[40] The investigations described below explore dislocations in shorter, yet isostructural, *n*-hexane,[41] *n*-octane[42,43] and *n*-decane,[44] chosen for reasons of computational economy.

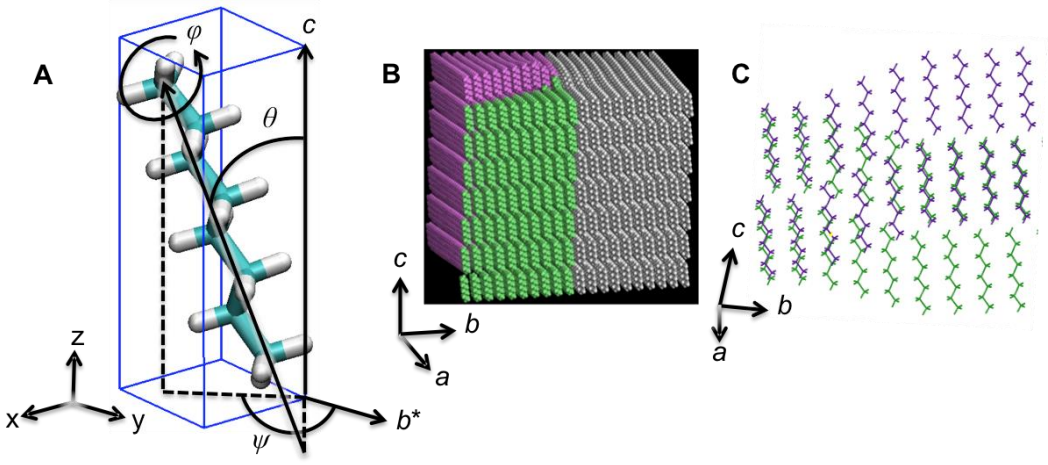

Figure 1. (A) *n*-Octane unit cell highlighting the azimuth orientation angle (ψ), inclination (θ), and axial angle (φ). (B) Shearing of perfect lattice yielding a single screw dislocation with **b** = ±1[001]. (C) Magnified section of slip interface illustrating previously predicted expectation[35,36,38] that chains would rise/fall two methylene units at a time to preserve zigzagging interdigitation of all-*anti* chains.

It was proposed[35,36,38] that dislocations in even *n*-alkane chains should be characterized by slips between chains in intervals of two methylene groups, such that the adjacent chains maintain registry with respect to the zigzag conformation (Fig. 1C). This mechanism suggests a straightforward analysis of the core structure that can be tested by computation. Simulation cells were built of optimized *n*-hexane (c_{exp} = 8.662 Å,[41] c_{opt} = 8.539 Å), *n*-octane (c_{exp} = 11.104 Å,[43] c_{opt} = 10.998 Å), and *n*-decane (c_{exp} = 13.586 Å,[44] c_{opt} = 13.507 Å) crystal structures (complete list of lattice parameters can be found in SI Table S2). Pairs of heterochiral screw dislocations were introduced into simulation cells to allow for the implementation of periodic boundary conditions (PBCs) during optimization and molecular dynamics

(MD) by shearing superlattices to yield Burgers vectors parallel to the dislocation line in the *c*-direction. The variable parameters of the starting configurations include: (*i*) the slip plane (*hkl*), (*ii*) screw handedness, (*iii*) separation between the two heterochiral cores *s*, (*iv*) the set-core radius *r**, equivalent to the distance in the *ab* plane over which the Burgers vector is traversed, and (*v*) the length of the Burgers vectors |**b**| (Fig. 2). The heterochiral dislocation pairs can be introduced as right (R) and left (L) handed (R/L), or the reverse (L/R), depending upon the side of the slip plane displaced along the +*c* direction (Figs. 2B, C). These alternative configurations are inequivalent for a triclinic system and must be evaluated independently.

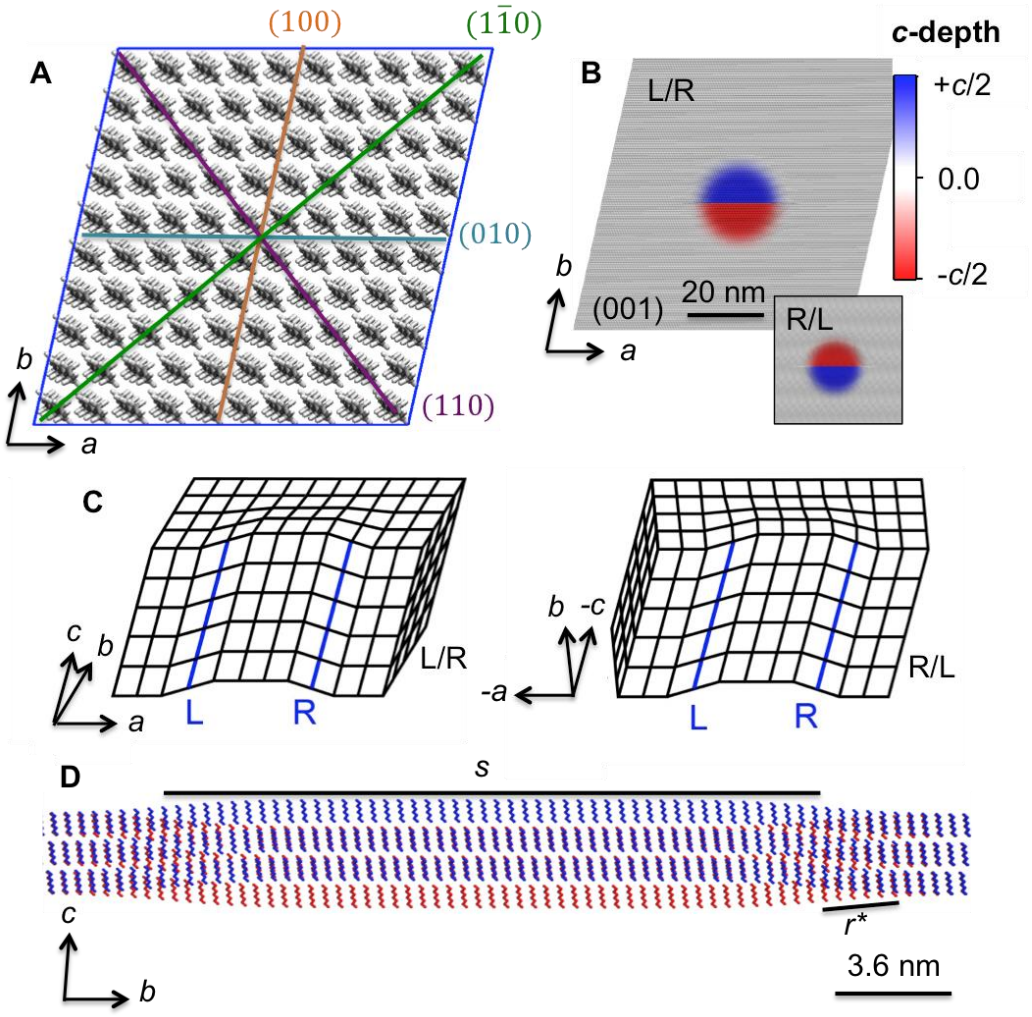

Figure 2. (A) *n*-Octane supercell as viewed normal to (001) denoting (100)[001], $(1\bar{1}0)$[001], (010)[001] and (110)[001] slip systems. (B) View of (001) for a lattice with a L/R heterochiral pair of dislocations generated by the (010)[001] slip system (inset: R/L (010)[001]). (C) L/R (left) and R/L (right) geometries are unique in a triclinic system. Note the supercell on the right was rotated around *a*. (D) View perpendicular to the slip plane of an initial sample lattice with a R/L heterochiral pair generated with the (010)[001] slip system, to highlight the separation between the two cores (*s*) and initial set-core radius (*r**).

Slip systems were evaluated initially by dislocating the lattice along the low index planes (100), (010), $(1\bar{1}0)$, and (110) (Fig. 2A). An initial set-core radius of 4**|b|** was used for all simulations, allowing for adequate dispersion of the initial strain. Heterochiral dislocations of **b** = ±1[001] in the (110) or (010) planes annihilate one another upon relaxation at temperatures within 20% of the melting point with separations ≤13**|b|**, the largest separation tested, whereas dislocations in the (100) and $(1\bar{1}0)$ planes persist (Figs. 3A – C). Core annihilation is accompanied by an increase in the length of the displaced interface in each of the adjacent cores, followed by a collapse of molecules at the slip plane to restore single crystal register under PBCs with displacements of either 0*c* or ±*Zc* where *Z* is an integer (SI Video S1). Dislocations in (100) or $(1\bar{1}0)$ planes are less mobile and the molecules become trapped in discrete structures of high strain and energy (SI Video S2) – even upon increasing the temperature of the simulation to 90% of the melting point – enabling investigation of the internal structures of the dislocation cores. The dislocation cores were highly anisotropic and elongated in (110) regardless of the slip system used to generate the pair (Figs. 4A, 5A). The elongated regions were visualized by plotting the difference in potential energy per molecule, with respect to the perfect lattice, averaged over the steady-state. Within the regions of elevated potential energy, there are small "hot spots" displaced to one side of the core, which is the locus of the dislocation.

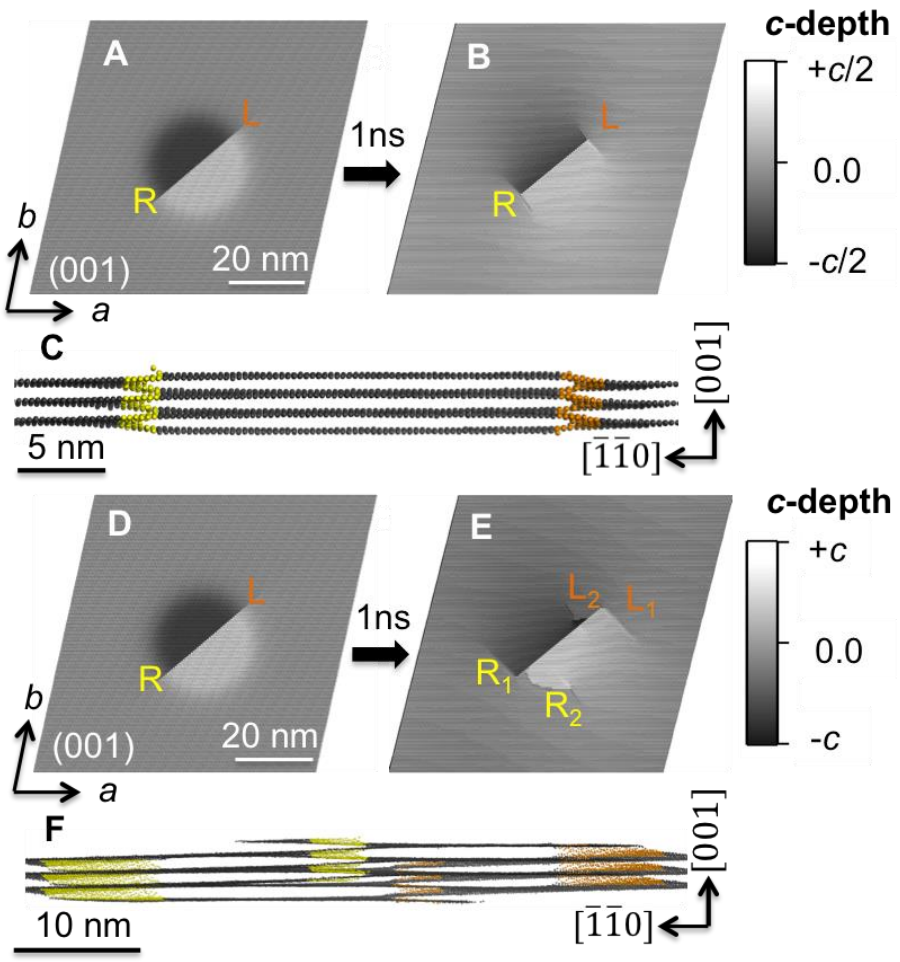

Figure 3. Displacements before optimization (A, D) and following MD (B, C, E, F) for R/L $(1\bar{1}0)[001]$ in *n*-octane with the molecules reduced to center of mass spheres and colored black to white according to *c*-depth (A, B, D, E) and yellow or orange for right- or left-handed sense (C, F). (A – C) When each dislocation in the heterochiral pair initially has **b** = ±1[001], the steady-state structure contains the two cores. (D – F) Dislocations in the heterochiral pair with initial **b** = ±2[001] result in a steady-state structure where the cores have split resulting in four cores, each with **b** = ±1[001]. (E) Mother/daughter cores labeled L_1/R_1 and L_2/R_2, respectively.

Given the low energy barrier for the cores to annihilate when introduced via the (010) and (110) slip planes, the Burgers vector was doubled, **b** = ±2[001]; however, the cores still annihilated even at low temperatures. Cores in the (100) and $(1\bar{1}0)$ with **b** = ±2[001] split into pairs with **b** = ± 1[001] at 90% of the melting point (SI Videos S3A, S3B). The four cores can be distinguished as mothers, positioned near

the original dislocations, and daughters displaced by 12.5 Å in the $[1\bar{1}0]$ (Figs. 3D - F and 5A). Dislocation dissociation is a common phenomenon and, for example, has been observed at the atomic level both experimentally[45] and by simulation[46] in silicon.

The initial R/L and L/R geometries (Fig. 2C) resulted in different steady-state structures following simulation only when the heterochiral dislocation pair was introduced with the (010)[001] slip system with an initial **b** = ±2[001]. The L/R pair was completely annihilated while the R/L pair was partially annihilated resulting in two discrete cores of **b** = ±1[001] that remained even when simulated at the highest temperatures (90% the melting point) for up to 5 ns (the longest simulation run). Additionally, subtle differences were also observed for cores in the (100) and $(1\bar{1}0)$ that split with the relative positions of the mother and daughter cores being opposite for the R/L and L/R structures.

The *z*-displacements u_z were used to evaluate strain (ε) according to linear elastic theory (Eq. 1).

$$\varepsilon_{xz} = \frac{1}{2}\frac{\partial u_z}{\partial x}, \varepsilon_{yz} = \frac{1}{2}\frac{\partial u_z}{\partial y} \quad (1)$$

Displacements in *x* and *y* with respect to *z* were omitted given their small magnitudes (<<0.01), as were the small ε_{xy}, ε_{xx}, ε_{yy} and ε_{zz} components. Strains ε_{xz} and ε_{yz} were calculated for the MD structures averaged over 350 frames spaced throughout the final 700 ps of the simulations (Figs. 4C, E). The strains were calculated between the centers of mass of neighboring molecules. For two dislocations in close proximity to one another, d_1 and d_2, centered as the hottest parts of the cores, ε_{xz} and ε_{yz} were expected according to isotropic elasticity (Eqs. 2, 3 and Figs. 4D, F).

$$\varepsilon_{xz}(x,y) = \frac{b}{4\pi}\left[\frac{y-y_{d1}}{(x-x_{d1})^2+(y-y_{d1})^2} - \frac{y-y_{d2}}{(x-x_{d2})^2+(y-y_{d2})^2}\right] \quad (2)$$

$$\varepsilon_{yz}(x,y) = \frac{b}{4\pi}\left[\frac{x-x_{d1}}{(x-x_{d1})^2+(y-y_{d1})^2} - \frac{x-x_{d2}}{(x-x_{d2})^2+(y-y_{d2})^2}\right] \quad (3)$$

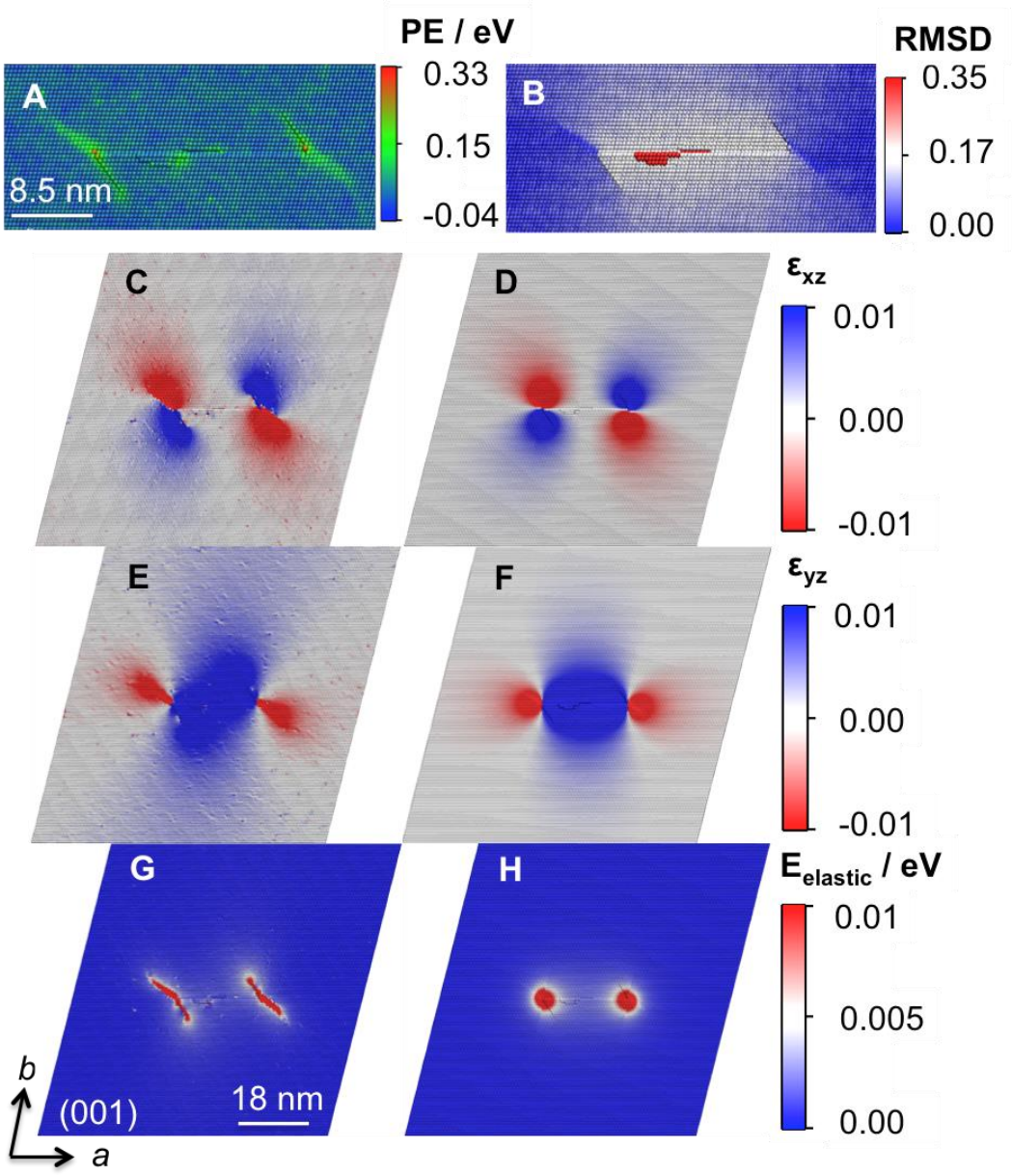

Figure 4. (A, B) The potential energy in eV and root-mean-square displacement (RMSD) plotted for each lattice position highlighting the two cores for R/L (010)[001] in *n*-octane with final **b** = ±1[001]. The strain tensor components, ε_{xz} and ε_{yz}, and the elastic energy $E_{elastic}$ for the computed results (C, E, G) compared to isotropic linear elastic theory (D, F, H) for the entire superlattice.

The resulting elastic energy was derived in the same way from the strain tensor elements ε_{xz} and ε_{yz} according to the atomistic simulations as well as the idealization based on the assumption of an

isotropic elastic medium according to equation (4), where W is the volume per molecule, approximated as the volume of the unit cell, and G is the calculated[47] shear modulus (Table 1 and Figs. 4G, H).

$$E_{\text{elastic}} = WG\left(\varepsilon_{xz}{}^2 + \varepsilon_{yz}{}^2\right) \qquad (4)$$

The values for elastic energy at the boundary of the simulation cell were very small, 0.6 to 1.9×10^{-5} (computational) and 0.7 to 1.4×10^{-5} (theoretical), indicating no substantial interactions between neighboring heterochiral pairs in the *ab* plane under PBCs.

Due to the highly anisotropic shape of the core, its size could not simply be estimated by plotting energy versus radius.[30,31] Two other approximate methods were used instead. The first one relied on the potential energy of the molecule. The sum of the average potential energy per molecule and the magnitude of its standard deviation in a perfect crystal was ca. 1.5 k_BT. The sharp change in the linear energy scale (Figs. 4A and 5A) occurs at twice this value and defines the core. Given that the cores resemble ellipses in shape, minor and major radii were measured parallel to [110] and $[1\bar{1}0]$, respectively (Table 1). The size was alternatively estimated by the strain distribution around the core. Cut-offs $|\varepsilon_{xz}| + |\varepsilon_{yz}|$ of 0.08, 0.05 and 0.03 for the *n*-octane core (Fig. 4) were used to measure major(minor) radii of 59(8), 68(9) and 80(11) Å, respectively. These major radii are longer than from the potential energy estimate, whereas the minor radii are comparable (i.e. strain cut-offs for the core resulted in even greater anisotropy). The major radii, which were measured along the crystallographic direction closest to the position of the long axis of the chains, also increased with chain length from *n*-hexane (32 Å) to *n*-decane (57 Å).

The energy of a dislocation $E_{\text{dislocation}}$ consists of two parts, the energy of the core E_{core} and the surrounding elastic regions E_{elastic}. Given equation (4), the energy of the core can be determined using equation (5), where PE_{perfect} and PE_{disloc} are the potential energies averaged over the steady-state portion of the simulation for the perfect lattice and the simulated cell after dislocating, respectively, m is the thickness of the simulation cell and E_{elastic} is approximated for all the molecules outside of the core

(Table 1). These values follow the approximate relationship $E_{core} = Gb^2/10$ (SI Fig. S2) indicating that elasticity is replaced by plastic deformations if elastic strain exceeds some threshold, $\varepsilon_c \approx 0.05$ (SI Fig. S3). In 1951, Frank had already estimated $\varepsilon_c \sim 0.1$.[48]

$$E_{\text{core}} = \frac{PE_{\text{disloc}} - PE_{\text{perfect}} - E_{\text{elastic}}}{m} \quad (5)$$

In *n*-hexane, *n*-octane, and *n*-decane, dislocation pairs with **b** = ±2[001] bifurcate to give four dislocations with **b** = ±1[001]. The energy of the latter are 1.5 – 2 times larger than that of cores initially set as **b** = ±1[001] (Table 1). Along with the complex distribution of residual displacements and potential energy (Fig. 5) this suggests the presence of additional interactions between these cores that preserve some of the extra energy associated with larger Burgers vectors.

Table 1. Characteristics of screw dislocations in *n*-alkanes.

n-Alkane	Energy cut-off, $3k_BT$ (eV)	Burgers vector, **b** = 1[001] (Å)	Shear modulus, *G* (GPa)	Minor radius, r_{minor} (Å)	Major radius, r_{major} (Å)	E_{core} (eV/Å)	$E_{double\ core}$ (eV/Å)[a]
Hexane	0.053	8.5	5.0	8(±1)	32(±3)	0.24(±0.11)	0.36(±0.07)
Octane	0.063	11.1	5.1	9(±2)	48(±7)	0.43(±0.09)	0.86(±0.05)
Decane	0.11	13.6	5.7	10(±1)	57(±7)	0.71(±0.09)	1.12(±0.21)

[a]Energy of a single core after splitting a pair of dislocations with **b** = ±2[001] to four dislocations with **b** = ±1[001]. The dislocation density in this case is doubled (7.0×14 m^{-2}) compared to the case of **b** = ±1[001] (3.5×14 m^{-2}).

It is well known that due to high elastic stress some dislocation cores are hollow.[49] Since molecules cannot escape a simulation with 3D periodic boundary conditions they may exhibit high mobility leading to quasi-liquid states in the core region. However, simulations show very low mobility of molecules even in the proximity of the dislocation line. The displacements of the centers of molecular masses with respect to the steady-state structure along *x*, *y* and *z* were ±0.38, 0.33 and 0.57 Å and ±0.24, 0.23 and 0.33 Å in the hottest part of the core and perfect region, respectively. Therefore, overall, the molecules in the core wandered 1.5 times more than in the perfect lattice. The average core energy density

$E_{core}/(\pi r_{minor} r_{major})$ = 0.30 – 0.40 meV/Å^3 is significantly lower than the heat of fusion 0.85 – 1.16 meV/Å^3 [50] and not enough to melt the core. Instead, inside the hottest part of the core there were *gauche* (0.19 meV/Å^3) conformations among the terminal C-C-C-C bonds (Fig. 5F). In the remainder of the core, molecules exhibit changes in molecular orientation rather than conformation. If molecules are viewed as vectors defined by the terminal carbons, an azimuthal orientation angle (ψ) between the *ab* projection of that vector and *b** and an angle of inclination (θ) between the vector and *c* (Figs. 1A and 5C, D) can be defined. The simulations revealed that θ and ψ decreased near the hottest part of the core as chains become more parallel to **b** and to *b**.

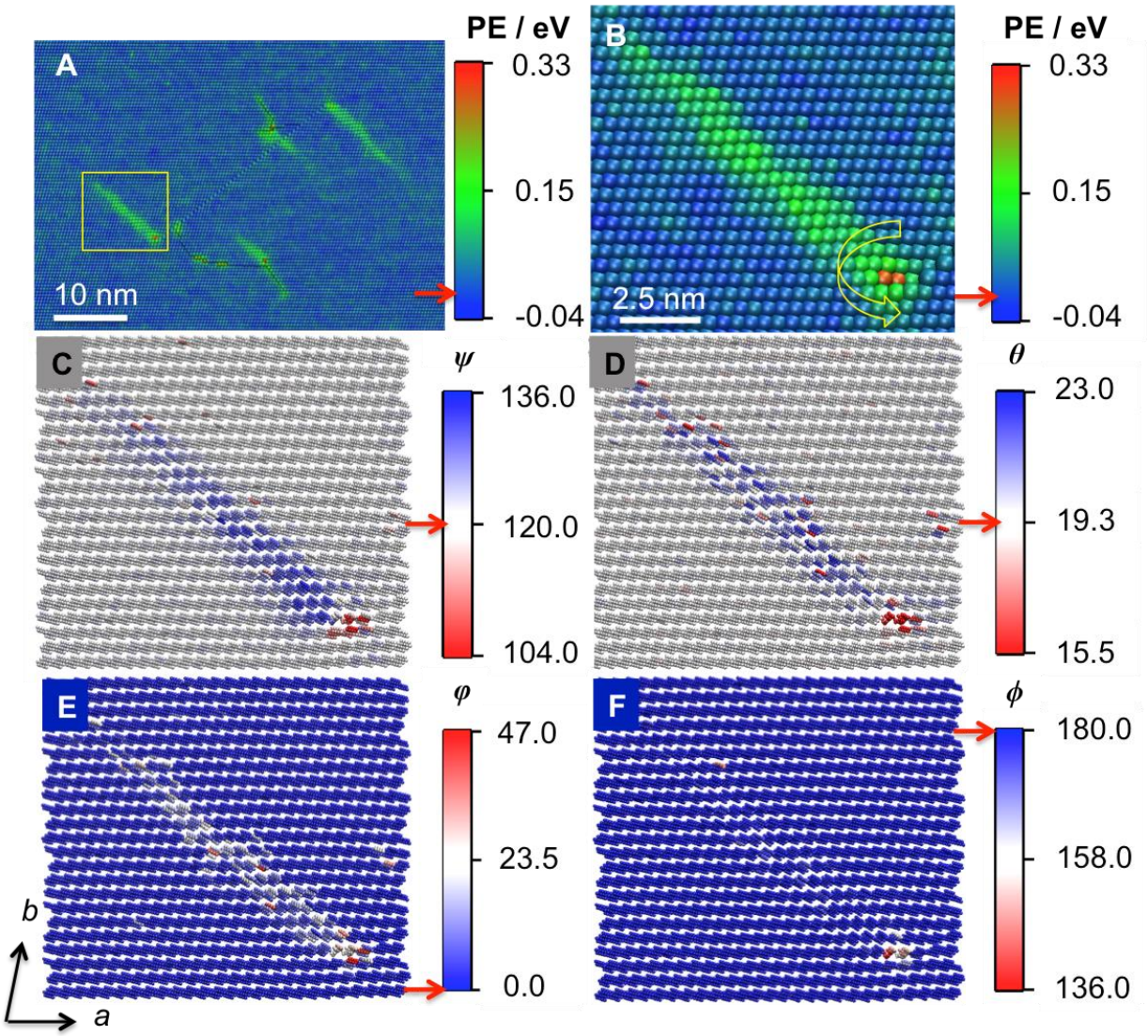

Figure 5. Potential energy per molecule in eV for R/L $(1\bar{1}0)[001]$ in *n*-octane following MD (Fig. 3E) with initial **b** = ±2[001] showing all four cores (A) and the yellow-boxed mother core (B) with **b** = ±1[001] highlighting the central "hot-spot" of high potential energy with the yellow arrow indicating the right-handed sense. The following were plotted per molecule for the core in (B) to elucidate the structure: (C) the azimuth orientation angle in degrees with respect to *b**, (D) inclination in degrees with respect to *c,* (E) the axial rotation of the molecule in degrees and (F) the average absolute value of the C-C-C-C dihedral angles in degrees. The values of the energy and angles for a perfect crystal region are denoted by the red arrow next to each scale bar. Details for the daughter core can be found in SI Fig. S5.

Lastly, we define the axial angle (φ) as the rotation of the best plane containing the carbon atoms in a single molecule (Figs. 1A and 5E). As mentioned above, it was proposed that slipping alkane chains should be displaced by successive lengths of two methylenes, until a Burgers vector is achieved.[35,36,38] This is expected for the zigzag packing of adjacent chains in these even *n*-alkanes. If displaced by odd numbers of methylenes, however, molecules can achieve interdigitation of zigzag chains by simply rotating 180° around their vector axis, thus flipping the orientation of the terminal C-C bonds relative to the perfect lattice (SI Fig. S4). The simulations performed here also reveal a variety of rotational values about the long molecular axis (φ) (Fig. 5E), indicating that the proposed two-methylene slip model is not as proscriptive as imagined in the early days of the screw dislocation concept since the molecules can rotate around their long axis to reduce the repulsive intermolecular interactions for out-of-phase, zigzagging slip events.

Atomistic simulations revealed that [001] screw dislocations in *n*-hexane, *n*-octane, and *n*-decane form elongated cores in (110) slip planes. These structures are manifest in maps of molecular potential energy as well as the orientations of the molecules with respect to the undisturbed lattice. At the locus of the dislocation, conformational distortions also were imposed. Outside the core, molecules undergo only *z*-displacements in agreement with the elastic stress field. Annihilation of heterochiral screw dislocations along easy (110) slip planes, and the splitting of high energy dislocations with exaggerated

Burgers vectors were animated. It is reasonable to suggest that motion on the (110) plane was the most facile owing to smaller energies associated with "molecular slip" along the long axes of the alkanes, a direct consequence of the alkane packing. Given the increasing demand for new tableted pharmaceuticals and crystalline organic electronic components, a first principles illustration of the structures, energies, and dynamics of dislocations presented herein is a first step to strategies for avoiding material failures that arise in plastic deformation.

Computational Methods: Optimizations and molecular dynamics (MD) employed the General Amber Force Field,[47] with a few *n*-octane dislocated structures simulated with the Condensed-phase Optimized Molecular Potentials for Atomistic Simulation Studies Force Field (COMPASS),[51] without any atomic charges to model the inter- and intra-molecular interactions at a range of finite temperatures relative to the calculated melting points to facilitate slip and traverse the energy landscape. All simulations were performed under periodic boundary conditions (PBCs) in the NPT ensemble for 1 ns with 1 fs time step and the LAMMPS code[52] without any molecular restraints.

AUTHOR INFORMATION

The authors declare no competing financial interests.

ACKNOWLEDGMENT

This work was primarily supported by the Materials Research Science and Engineering Center (MRSEC) program of the National Science Foundation under award number DMR-1420073. I.O. was supported in part through a Margaret Kramer Fellowship. Funding was also provided by the Australian Research Council (grants FT130100463 and DP140101776). This work was supported by computational resources

provided by the Australian Government through the Pawsey Centre under the National Computational Merit Allocation Scheme.

Supporting Information Available: Additional computational methodology details on the melting point determination, simulation cell construction with the code to generate such structures available at http://dx.doi.org/10.5281/zenodo.58258, shear modulus calculations, and the Frank Radius approximations, force field parameters, comparison between simulated and experimental lattice parameters, comparison between simulated dislocations employing GAFF and COMPASS, comparison of calculated core energies and elastic strain boundaries for the even *n*-alkanes to materials previously reported, further detailed description of the importance of the axial angle (φ), and the daughter core structure for comparison to mother core (Fig. 5). (PDF)
Animations of the dislocation pair dynamics with various |**b**| (SI Videos S1, S2, S3A, and S3B *.mov).

REFERENCES

(1) Leterrier, Y. Mechanics of Curvature and Strain in Flexible Organic Electronic Devices. In *Handbook of Flexible Organic Electronics*; Logothetidis, S., Ed.; Woodhead Publishing: Cambridge, U.K., 2015; pp 3-36.

(2) Sun, C. C. Decoding Powder Tabletability: Roles of Particle Adhesion and Plasticity. *J. Adhes. Sci. Technol*. **2011**, *25,* 483-499.

(3) Chapman, B. D.; Checco, A.; Pindak, R.; Siegrist, T.; Kloc, C. Dislocations and Grain Boundaries in Semiconducting Rubrene Single-Crystals. *J. Cryst. Growth* **2006**, *290*, 479-484.

(4) Witte, G.; Hänel, K.; Söhnchen, S.; Wöll, Ch. Growth and Morphology of Thin Films of Aromatic Molecules on Metals: The Case of Perylene. *Appl. Phys. A*. **2006**, *82*, 447-455.

(5) Jones, W.; Eddleston, M. D. *Disordered Pharmaceutical Materials*; Descamps, M., Ed.; Wiley-VCH: Weinheim, 2016; pp 103-134.

(6) Lei, L.; Carvajal, T.; Koslowski, M. Defect-Induced Solid State Amorphization of Molecular Crystals. *J. Appl. Phys*. **2012**, *111*, 073505.

(7) Reddy, C.M.; Krishna, G.R.; Ghosh, S. Mechanical Properties of Molecular Crystals – Applications to Crystal Engineering. *CrystEngComm* **2010**, *12*, 2296–2314.

(8) Naumov, P.; Chizhik, S.; Panda, M. K.; Nath, N. K.; Boldyreva, E. Mechanically Responsive Molecular Crystals. *Chem. Rev*. **2015**, *115*, 12440–12490.

(9) Bulatov, V.; Cai, W. *Computer Simulations of Dislocations*; Oxford University Press: New York, 2006.

(10) Zhang, F.; Walker, A. M.; Wright, K.; Gale, J. D. Defects and Dislocations in MgO: Atomic Scale Models of Impurity Segregation and Fast Pipe Diffusion. *J. Mater. Chem*. **2010**, *20*, 10445–10451.

(11) Spence, J. C. H. *Experimental High-Resolution Electron Microscopy*, 3rd ed.; Oxford University Press: New York, 2003.

(12) Hirsch, P. B.; Cockayne, D. J. H.; Spence, J. C. H.; Whelan, M. 50 Years of TEM of Dislocations: Past, Present and Future. *J. Phil. Mag*. **2006**, *86*, 4519–4528.

(13) Mokichev, N. N.; Pakhomov, L. G. Computer-Simulation of Edge Dislocation in Naphthalene Crystals. *Sov. Phys. Solid State* **1982**, *24*, 3389.

(14) Dick, J. J.; Ritchie, J. P. Molecular Mechanics Modeling of Shear and the Crystal Orientation Dependence of the Elastic Precursor Shock Strength in Pentaerythritol Tetranitrate. *J. Appl. Phys*. **1994**, *76*, 2726-2737.

(15) Mathew, N.; Picu, C. R.; Chung, P. J. Peierls Stress of Dislocations in Molecular Crystal Cyclotrimethylene Trinitramine. *Phys. Chem. A* **2013**, *117*, 5326-5334.

(16) Munday, L. B.; Mitchell, R. L.; Knap, J.; Chung, P. W. Role of Molecules Flexibility on the Nucleation of Dislocations in Molecular Crystals. *Appl. Phys. Lett*. **2013**, *103*, 151911.

(17) Jaramillo, E.; Sewell, T. D.; Strachan, A. Atomic-Level View of Inelastic Deformation in a Shock Loaded Molecular Crystal. *Phys. Rev. B* **2007**, *76*, 064112.

(18) Cawkwell, M. J.; Ramos, K. J.; Hooks, D. E.; Sewell, T. D. Homogeneous Dislocation Nucleation in Cyclotrimethylene Trinitramine Under Shock Loading. *J. Appl. Phys*. **2010**, *107*, 063512.

(19) Bacon, D. J.; Tharmalingam, K. Computer Simulation of Polyethylene Crystals: Part 3, the Core Structure of Dislocations. *J. Mater. Sci*. **1983**, *18*, 884-893.

(20) Musienko, A. I.; Balabaev, N. K.; Manevitch L. I. Modeling of Screw Dislocation Dynamics in Crystalline Polyethylene. *Dokl. Phys. Chem.* **2002**, *384*, 213-215.

(21) Tamaki, S.; Ide, N.; Okada, I.; Kojima, K. Computer Simulation of Core Structure of Screw Dislocations in C_{60} Crystals Using Girifalco Potential. *Jap. J. Appl. Phys*. **1998**, *37*, 2608-2609.

(22) Pal, A.; Picu, C. R. Rotational Defects in Cyclotrimethylene Trinitramine (RDX) Crystals. *J. Chem. Phys*. **2014**, *140*, 044512.

(23) Ide, N.; Okada, I.; Kojima, K. Computer Simulation of Core Structure and Peierls Stress of Dislocations in Anthracene Crystals. *J. Phys. Condens. Matter* **1993**, *5*, 3151-3162.

(24) Lei, L.; Koslowski, M. Mesoscale Modeling of Dislocations in Molecular Crystals. *Phil. Mag*. **2011**, *91*, 865-878.

(25) Walker, A. M.; Gale, J. D.; Slater, B.; Wright, K. Atomic Scale Modelling of the Cores of Dislocations in Complex Materials Part 1: Methodology. *Phys. Chem. Chem. Phys*. **2005***, 7*, 3227-3234.

(26) Walker, A. M.; Gale, J. D.; Slater, B.; Wright, K. Atomic Scale Modelling of the Cores of Dislocations in Complex Materials Part 2: Applications. *Phys. Chem. Chem. Phys*. **2005***, 7*, 3235-3242.

(27) Walker, A. M.; Slater, B.; Gale, J. D.; Wright, K. Predicting the Structure of Screw Dislocations in Nanoporous Materials. *Nat. Mater*. **2004**, *3*, 715-720.

(28) Walker, A. M.; Slater, B. Comment Upon the Screw Dislocation Structure on HKUST-1 {111} Surfaces. *Cryst. Eng. Comm.* **2008**, *10*, 790-791.

(29) Walker, A. M.; Carrez, P.; Cordier, P. Atomic-Scale Models of Dislocation Cores in Minerals: Progress and Prospects. *Miner. Mag*. **2010**, *74,* 381-413.

(30) Walker, A. M. Simulation of Screw Dislocations in Wadsleyite. *Phys. Chem. Minerals* **2010**, *37*, 301-310.

(31) Shahsavari, R.; Chen, L. Screw Dislocations in Complex, Low Symmetry Oxides: Core Structures, Energetics, and Impact on Crystal Growth. *Appl. Mater. Interfaces* **2015**, *7*, 2223-2234.

(32) Kitaigorodsky, A. I. *Molecular Crystals and Molecules*; Academic Press: New York, 1973.

(33) Amelinckx, S. Growth Features on Crystals of Long-Chain Compounds. III. *Acta. Cryst*. **1956**, *9*, 217-224.

(34) Boistelle, R.; Simon, B.; Pepe, G. Polytypic Structures of *n*-$C_{28}H_{58}$ (Octacosane) and *n*-$C_{36}H_{74}$ (Hexatriacontane). *Acta. Cryst*. **1976**, *B32*, 1240-1243.

(35) Dawson, I. M.; Vand, V. The Observation of Spiral Growth-Steps in Normal-Paraffin Single Crystals in the Electron Microscope. *Proc. Roy. Soc. London Series A. Math. Phys. Sci.* **1951,** *205*, 555-562.

(36) Anderson, N. G.; Dawson, I. M. The Study of Crystal Growth with the Electron Microscope. III. Growth-Step Patterns and the Relationship of Growth-Step Height to Molecular Structure in *n*-Nonatriacontane and in Stearic Acid. *Proc. Roy. Soc. London, Series A. Math. Phys. Sci*. **1953**, *218*, 255-268.

(37) Plomp, M.; van Enckevort W.J.P.; van Hoof, P.J.C.M.; van de Streek, C.J. Morphology of and Dislocation Movement in *n*-$C_{40}H_{82}$ Paraffin Crystals Grown from Solution. *J. Cryst. Growth* **2003**, *249*, 600-613.

(38) Dawson, I. M. The Study of Crystal Growth with the Electron Microscope. II. The Observation of Growth Steps in the Paraffin *n*-Hectane. *Proc. Roy. Soc. London Series A. Math. Phys. Sci.* **1952**, *214*, 72-79.

(39) Craig, S. R.; Hastie, G. P.; Roberts, K. J.; Sherwood, J. N. Investigation into the Structures of Some Normal Alkanes within the Homologous Series $C_{13}H_{28}$ to $C_{60}H_{122}$ Using High-Resolution Synchrotron X-ray powder Diffraction. *J. Mater. Chem*. **1994**, *4*, 977-981.

(40) Turner, W. R. Normal Alkanes. *Ind. Eng. Prod. Res. Dev*. **1971**, *10*, 238-260.

(41) Norman, N.; Mathisen, H. The Crystal Structure of Lower *n*-Paraffins. II. *n*-Hexane. *Acta Chimica Scand*. **1961**, *15*, 1755-1760.

(42) Mathisen, H.; Norman, N.; Pedersen, B. F. Crystal Structure of Lower Paraffins. IV. Refinement of Crystal Structures of Pentane and Octane. *Acta Chimica Scand*. **1967**, *21*, 127-135.

(43) Boese, R.; Weiss, H.-C.; Blaeser, D. The Melting Point Alternation in the Short-Chain *n*-Alkanes: Single-Crystal x-Ray Analyses of Propane at 30K and of *n*-Butane to *n*-Nonane at 90 K. *Angew. Chem. Int. Ed*. **1999**, *38*, 988-992.

(44) Bond, A. D.; Davies J. E. *n*-Decane. *Acta Cryst*. **2002**, *E58*, o196-o197.

(45) Belov, A. Y.; Scholz, R.; Scheerschmidt K. Dissociation of Screw Dislocations in (001) Low-Angle Twist Boundaries: A Source of the 30^{o} Partial Dislocations in Silicon. *Phil. Mag. Lett.* **1999**, *79*, 531 – 538.

(46) Pizzagalli, L. Atomistic Modeling of the Dissociation of a Screw Dislocation in Silicon. *J. Mater. Sci*. **2016**, *51*, 2869-2876.

(47) Wang, J.; Wolf, R. M.; Caldwell, J. W.; Kollman, P. A.; Case, D. A. Development and Testing of a General Amber Force Field. *J. Comput. Chem*. **2004**, *25*, 1157-1174, errata, **2005**, *26*, 114.

(48) Frank, F. C. Capillary Equilibria of Dislocated Crystals. *Acta Cryst*. **1951**, *4*, 497-501.

(49) van der Hoek, B.; van der Eerden, J.P.; Bennema, P. Thermodynamic Stability Conditions for the Occurrence of Hollow Cores Caused by Stress of Line and Planar Defects. *J. Cryst. Growth* **1982**, *56*, 621-632.

(50) Acree, W. E. Jr. Thermodynamic Properties of Organic Compounds: Enthalpy of Fusion and Melting Point Temperature Compilation. *Thermochim. Acta* **1991**, *189*, 37-56.

(51) Sun, H. COMPASS: An ab initio Force-Field Optimized for Condensed-Phase Applications – Overview with Details on Alkane and Benzene Compounds. *J. Phys. Chem. B* **1998**, *102*, 7338-7364.

(52) Plimpton, S. Fast Parallel Algorithms for Short-Range Molecular Dynamics. *J. Comput. Phys.* **1995**, *117*, 1-19.